Biallelic Mutations in *LIPT2* Cause a Mitochondrial Lipoylation Defect Associated with Severe Neonatal Encephalopathy

Florence Habarou,[1,2,20] Yamina Hamel,[1,3,20] Tobias B. Haack,[4,5,6,20] René G. Feichtinger,[7] Elise Lebigot,[8] Iris Marquardt,[9] Kanetee Busiah,[1] Cécile Laroche,[10] Marine Madrange,[1,3] Coraline Grisel,[1] Clément Pontoizeau,[1,2] Monika Eisermann,[11] Audrey Boutron,[8] Dominique Chrétien,[3] Bernadette Chadefaux-Vekemans,[1,2] Robert Barouki,[1,2] Christine Bole-Feysot,[12] Patrick Nitschke,[13] Nicolas Goudin,[1,11] Nathalie Boddaert,[14] Ivan Nemazanyy,[15,16] Agnès Delahodde,[17] Stefan Kölker,[18] Richard J. Rodenburg,[19] G. Christoph Korenke,[9] Thomas Meitinger,[4,5] Tim M. Strom,[4,5] Holger Prokisch,[4,5] Agnes Rotig,[3] Chris Ottolenghi,[1,2] Johannes A. Mayr,[7,20,*] and Pascale de Lonlay[1,3,20,*]

Lipoate serves as a cofactor for the glycine cleavage system (GCS) and four 2-oxoacid dehydrogenases functioning in energy metabolism (α-oxoglutarate dehydrogenase [α-KGDHc] and pyruvate dehydrogenase [PDHc]), or amino acid metabolism (branched-chain oxoacid dehydrogenase, 2-oxoadipate dehydrogenase). Mitochondrial lipoate synthesis involves three enzymatic steps catalyzed sequentially by lipoyl(octanoyl) transferase 2 (LIPT2), lipoic acid synthetase (LIAS), and lipoyltransferase 1 (LIPT1). Mutations in *LIAS* have been associated with nonketotic hyperglycinemia-like early-onset convulsions and encephalopathy combined with a defect in mitochondrial energy metabolism. LIPT1 deficiency spares GCS deficiency and has been associated with a biochemical signature of combined 2-oxoacid dehydrogenase deficiency leading to early death or Leigh-like encephalopathy. We report on the identification of biallelic *LIPT2* mutations in three affected individuals from two families with severe neonatal encephalopathy. Brain MRI showed major cortical atrophy with white matter abnormalities and cysts. Plasma glycine was mildly increased. Affected individuals' fibroblasts showed reduced oxygen consumption rates, PDHc, α-KGDHc activities, leucine catabolic flux, and decreased protein lipoylation. A normalization of lipoylation was observed after expression of wild-type LIPT2, arguing for LIPT2 requirement in intramitochondrial lipoate synthesis. Lipoic acid supplementation did not improve clinical condition nor activities of PDHc, α-KGDHc, or leucine metabolism in fibroblasts and was ineffective in yeast deleted for the orthologous *LIP2*.

Lipoic acid (LA) is an essential cofactor of major mitochondrial enzyme complexes (Figure S1), including the glycine cleavage system (GCS) and four 2-oxoacid dehydrogenases, namely pyruvate dehydrogenase (PDHc; pyruvate oxidation), α-oxoglutarate dehydrogenase (α-KGDHc; Krebs cycle), branched chain α-oxoacid dehydrogenase (BCKDHc; leucine, isoleucine, and valine catabolism), and 2-oxoadipate dehydrogenase (2-OADH, lysine catabolism). This cofactor is covalently bound to a conserved lysine residue of the E2 subunits of PDHc, BCKDHc, 2-OADH, and α-KGDHc as well as the H protein of GCS. In addition, lipoylation of the E3-binding protein (E3BP) of PDHc has been observed. Based on studies in yeast, the LA biosynthesis pathway involves mitochondrial fatty acid synthesis up to eight carbon length (octanoyl moiety bound to an acyl carrier protein, ACP) and three lipoate-specific sequential enzymes, LIPT2, LIAS, and LIPT1.[1–5] In brief, LIPT2 transfers an octanoyl moiety from octanoyl-ACP on the GCS H protein, LIAS adds two sulfur atoms to produce a lipoyl residue, and LIPT1 transfers lipoyl residues from the GCS H protein to the E2 subunits of PDHc, BCKDHc, 2-OADH, and α-KGDHc (Figure S1).

We and others have recently shown that mutations involving *LIAS* (MIM: 614462) and *LIPT1* (MIM: 616299)

[1]Reference Center of Inherited Metabolic Diseases, University Paris Descartes, Hospital Necker Enfants Malades, APHP, 75015 Paris, France; [2]Metabolic Biochemistry, University Paris Descartes, Hospital Necker Enfants Malades, 75015 Paris, France; [3]UMR1163, University Paris Descartes, Sorbonne Paris Cité, Institut IMAGINE, 24 Boulevard du Montparnasse, 75015 Paris, France; [4]Institute of Human Genetics, Technische Universität München, 81675 Munich, Germany; [5]Institute of Human Genetics, Helmholtz Zentrum München, 85764 Neuherberg, Germany; [6]Institute of Medical Genetics and Applied Genomics, University of Tübingen, 72076 Tübingen, Germany; [7]Department of Pediatrics, Paracelsus Medical University Salzburg, 5020 Salzburg, Austria; [8]Department of Biochemistry, Hospital Bicêtre, APHP, 94270 Le Kremlin Bicêtre, France; [9]Department of Neuropediatrics, Children's Hospital Klinikum Oldenburg, Oldenburg 26133, Germany; [10]Neurology Unit, Limoges Hospital, 87042 Limoges, France; [11]Neurophysiology Unit, Hospital Necker Enfants Malades, APHP, 75015 Paris, France; INSERM U1129, Paris, France; Paris Descartes University; CEA, Gif sur Yvette; Paris, France; [12]Genomic Core Facility, Imagine Institute, UMR1163, University Paris Descartes, 24 Boulevard du Montparnasse, 75015 Paris, France; Hospital Necker Enfants Malades, APHP, 75015 Paris, France; [13]Paris Descartes Bioinformatic Platform, University Paris Descartes, Hospital Necker Enfants Malades, 75015 Paris, France; [14]Department of Pediatric Radiology, Hospital Necker Enfants Malades, AP-HP, University René Descartes, PRES Sorbonne Paris Cité, INSERM U1000, Institut Imagine 24 Boulevard du Montparnasse, 75015 Paris, France; [15]Faculty of Medicine, Paris Descartes University, Paris 75015, France; [16]Necker Enfants Malades Institute, INSERM U1151, Paris Descartes University, 75015 Paris, France; [17]Institute for Integrative Biology of the Cell (I2BC), CEA, CNRS, University Paris-Sud, Université Paris-Saclay, 91198 Gif-sur-Yvette Cedex, France; [18]Department of General Pediatrics, Division of Pediatric Neurology and Inherited Metabolic Diseases, University Children's Hospital, 69120 Heidelberg, Germany; [19]Radboud Center for Mitochondrial Medicine, Department of Pediatrics, Radboud UMC, Nijmegen, the Netherlands
[20]These authors contributed equally to this work
*Correspondence: h.mayr@salk.at (J.A.M.), pascale.delonlay@aphp.fr (P.d.L.)
http://dx.doi.org/10.1016/j.ajhg.2017.07.001.
© 2017 American Society of Human Genetics.

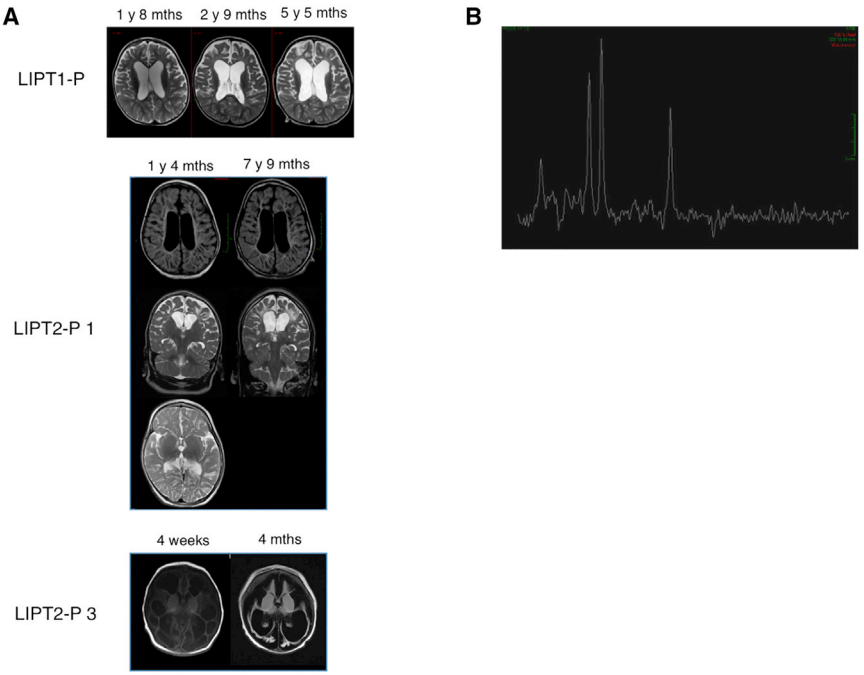

Figure 1. Brain MRI and MRS Spectroscopy

(A) Brain MRIs of individuals with *LIPT1* and *LIPT2* mutations. As in LIPT1-deficient individual (LIPT1-P, top), brain MRI revealed supra-tentorial cortical atrophy, ventricular dilatation in P1 with LIPT2 deficiency (LIPT2-P1, middle), cortical anomalies with cystic white matter anomalies at age 4 weeks, and major cortical and subcortical atrophy with ventricular dilatation and formation of major cysts at age 4 months in P3 with LIPT2 deficiency (LIPT2-P3, bottom).

(B) MRS spectroscopy in P1 with LIPT2 deficiency. MRS spectroscopy with long TE showed a peak of lactate (1.3 ppm).

lead to severe clinical conditions.[6–8] Because LIAS is an iron-sulfur cluster (ISC) protein, lipoylation deficiency is a prominent feature of defective iron-sulfur [4Fe-4S] cluster cofactor biosynthesis (e.g., *NFU1* [MIM: 605711], *BOLA3* [MIM: 614299], *IBA57* [MIM: 615330], *LYRM4* [MIM: 615595][9–15]). ISC cofactors also participate in electron transfer reactions and are required for respiratory chain complexes I, II, and III,[16,17] thereby accounting for combined lipoic acid and OXPHOS deficiency.[11,18] Furthermore, defects in mitochondrial transport of S-adenosylmethionine (SAM), mediated by SLC25A26, result in defective LA synthesis, since SAM is a substrate for the lipoic acid synthetase (MIM: 616794).[19] Here we report on three individuals from two unrelated families (Figure S2) with a lipoate-related disease involving α-oxoacid dehydrogenase dysfunction due to mutations in *LIPT2*, encoding the enzyme that catalyzes the first dedicated step of the LA biosynthesis pathway. This study was approved by the local ethics committees. Informed consent was obtained from the parents.

Individuals presented with severe neonatal-onset encephalopathy and abnormal EEG summarized in the Supplemental Note (see also Figure S3 and Table S1). Both clinical and radiological findings were reminiscent of LIPT1 deficiency,[7,8] whereas first-line biochemical findings were abnormal yet little specific.

Individual P1 is alive with no episodes of metabolic decompensation. Brain MRI showed marked supra-tentorial cortical atrophy with ventricular dilatation, bi-frontal white matter abnormalities, and delayed myelination (Figure 1A, middle), similar to those observed in a previously described LIPT1-deficient individual[7] (Figure 1A, top). MRS spectroscopy with a long TE (144) showed a lactate peak (Figure 1B). Laboratory testing showed hyperlactatemia with a high lactate/pyruvate ratio at 16 months of age, but CSF lactate was normal as well as bicarbonates and urinary organic acid analysis except for a slight increase in lactate (Table S2). Moderate biochemical abnormalities in plasma amino acids included moderate hyperglycinemia contrary to LIPT1 deficiencies previously described,[7,8] increased alanine and decreased branched-chain amino acids (Table S2). At that time, these results were not suggestive of combined α-oxoacid dehydrogenase deficiency or E3 deficiency (MIM: 246900) but rather suggested denutrition. During follow-up, the lactate levels normalized (age 5 years). As in LIPT1 deficiency,[7,8] no elevations were noted for α-hydroxy or α-oxoadipic acids, thus contrasting with the large increases and sometimes massive amounts observed in typical forms of NFU1 deficiency.[9] Mitochondrial respiratory chain activities in skeletal muscle and liver and E3 subunit activity measured in fibroblast homogenates were normal (data not shown).[20] Using blood DNA, Sanger sequencing did not identify pathogenic gene variations in *PDHA1* (MIM: 312170), *PDHB* (MIM: 614111), *PDHX* (MIM: 245349), *DLAT* (MIM: 245348), *DLD*,[21] *LIAS*, *BOLA3*, *NFU1*, and *LIPT1*. Subsequently, exome sequencing was performed as previously described[7] and resulted in a list of 35 candidate genes, including only one encoding a mitochondrial protein, LIPT2. In P1, the two heterozygous c.89T>C transition and c.377T>G transversion were found in *LIPT2* (GenBank: NM_001144869.2; see below). To ensure that *LIPT2* mutations led to a decrease in lipoic-acid-dependent enzymatic activities, we measured oxygen consumption using pyruvate as a substrate and PDHc and α-KGDHc activities in fibroblasts.[22] Both metabolic investigations were severely reduced (Tables S3 and S4) as in LIPT1-deficient individual.[7] In P1 fibroblasts, consistent with a defect in both the Krebs' cycle and PDHc activity, 1 mmol/L $^{13}C_5$-labeled glutamine loading test revealed decreased fumarate versus normal proline labeling (Figure 2A), and 1 mmol/L $^{13}C_6$-labeled leucine loading test (a modification

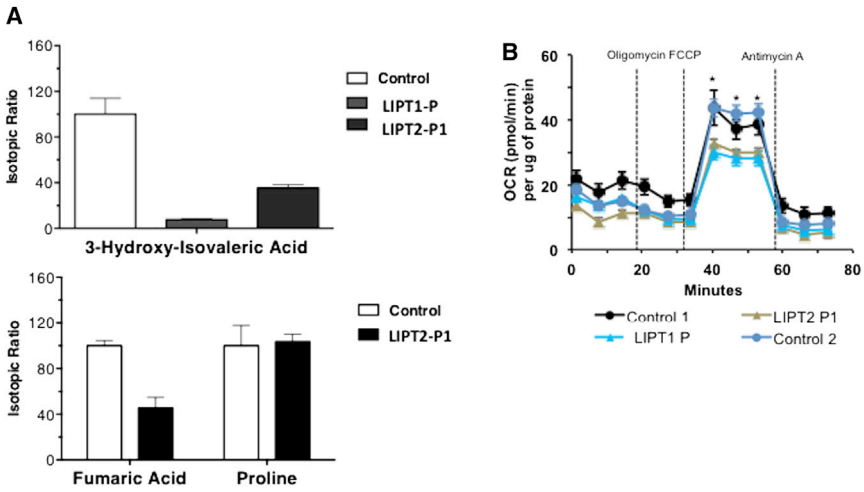

Figure 2. Labeled Glutamine and Leucine Loading Tests and Oxygen Consumption Rates in Fibroblasts from Control Subjects and Individuals with LIPT1 and LIPT2 Deficiencies

(A) Labeled to natural ratios for 3-hydroxyisovaleric acid after a $^{13}C_6$ leucine loading test in fibroblasts of an individual with LIPT1 deficiency and LIPT2-P1 and for fumaric acid and proline after a $^{13}C_5$ glutamine loading test in LIPT2-P1 and control fibroblasts. Labeled leucine and glutamine loading tests are consistent with decreased BCKDHc activity and Krebs cycle activity defects. Labeled amino acids were acquired from Eurisotop. Organic acids derived from labeled substrates were measured by gas chromatography-mass spectrometry (GC-436 Scion-TQD, Brüker Daltonics). Results are presented as means ± SD of triplicates.

(B) Oxygen consumption rates measured in fibroblasts from healthy subjects and individuals with LIPT1 and LIPT2 deficiencies. Basal OCR levels did not differ significantly in fibroblasts from healthy control subjects and individuals with LIPT1[7] and LIPT2 deficiencies. By contrast, when challenged with a mitochondrial uncoupler (FCCP), fibroblasts from healthy individuals responded with the expected increase in oxygen consumption, whereas the response in cells from individuals with LIPT1 and LIPT2 deficiency was significantly lower. OCR was measured using the XF Cell Mito Stress Test Kit and XFe96 analyzer (Seahorse Bioscience, Agilent Technologies) following the manufacturer's protocols.[23] Cells were seeded at the density 30,000 cells/well in an XFe96cell culture microplate and allowed to attach for 3 hr before the measurement. Basal OCR was measured, followed by sequential treatment with Oligomycin A (1 μM), FCCP (1 μM), and Antimycin A (1 μM). Each treatment was measured every 3 min (3 min measurement) three times and a minimum of six replicates were utilized per condition. All compounds and materials were obtained from Seahorse Bioscience. Protein concentrations in each well were determined with the BCA method (Pierce) in cell lysates after the measurement. Data are presented as mean ± SEM normalized to protein content in each well. Statistical test was performed using ANOVA test; *$p \leq 0.05$ control versus affected individuals' cells.

of a previously described radioactive test[24]) revealed decreased BCKDHc activity, but to a lesser extent than in LIPT1-deficient individual (Figure 2A). Lipoic acid administration was orally tested over 3 months at a daily dosage of 25 mg/kg/day in two doses. No clinical modification was observed by the parents, and the neurological examination remained unchanged.

Individuals P2 and P3, two siblings whose healthy parents are of German origin, died in the first year of life without any psychomotor acquisition (see Supplemental Note). Lactate concentration of individual P2 was 3.7 mmol/L at birth and increased to values between 8 and 10, in a single measurement up to 111 mmol/L (N < 1.8 mmol/L). Brain MRI showed periventricular cystic changes. A ketogenic diet was started, which resulted in a decrease of lactate concentrations but also led to a weight loss and worsening of his condition. Organic acids in urine were elevated (Table S2). Biochemical investigations in fibroblasts found decreased PDHc activity (Table S3) while respiratory chain enzyme activities were normal (data not shown). Individual P3 presented with severe lactic acidosis up to 17 mmol/L at birth. Brain MRI showed enlarged lateral ventricles and formation of cysts in the cortex and white matter of the whole cerebral structures. Furthermore, gyration of the cerebral hemispheres was decreased (Figure 1A, bottom). Metabolite investigations showed elevated lactate concentrations in blood and cerebrospinal fluid and elevated pyruvate in blood, with a lactate/pyruvate ratio of 30 (N < 20) (Table S2). Amino acid analysis in plasma showed elevation of alanine and proline, moderate increase of glycine, and decrease of branched-chain amino acids (Table S2). Investigation of organic acids in urine revealed elevation of lactate, pyruvate, and 2-oxoglutarate. A muscle biopsy performed at the age of 2 weeks revealed some variability in fiber diameters (7–19 μm) but no ragged-red or cytochrome *c* oxidase negative fibers. Electron microscopy showed some subsarcolemnal glycogen accumulation but normal structure of mitochondria. The activity of respiratory chain enzymes complexes I, II, III, and IV was normal (data not shown). Investigation of pyruvate dehydrogenase in fibroblasts was decreased (Table S3).

In P2, panel diagnostics for gene mutations associated with mitochondrial diseases was performed but did not reveal any abnormal result. Exome sequencing, performed as previously described,[25–27] revealed compound heterozygous mutations in *LIPT2* c.314T>G (p.Leu105Arg; not reported in gnomAD) and c.377T>G (p.Leu126Arg; frequency reported in gnomAD: 0.0001878), the latter being shared with P1. Sanger sequencing confirmed mutations in P1, P2, and P3 and showed that the parents were heterozygous for one of these mutations. The mutations c.314T>G and c.377T>G were predicted to be "probably damaging" by PolyPhen-2 (Table S5) and were located in a conserved domain of the protein (Figure S2). The c.89T>C variation is a SNP (rs539962457, minor allele frequency [MAF] < 0.0002/1; frequency reported in gnomAD: 0.00003238). It changes a leucine into a proline (p.Leu30Pro) at the second last position of a conserved alpha-helix, which is the predicted mitochondrial targeting sequence of LIPT2 protein and was considered as "possibly damaging" by PolyPhen. These variations were not found in more than

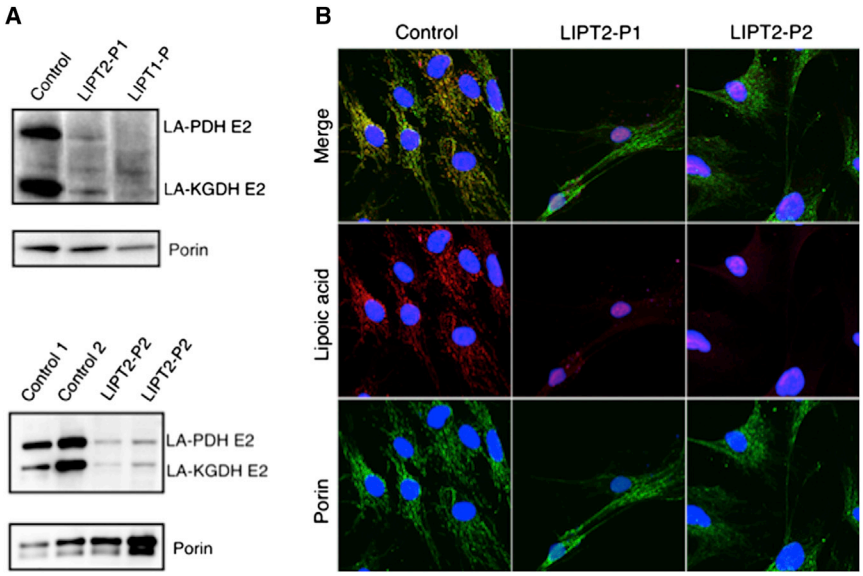

Figure 3. Immunoblot and Immunofluorescence Staining of Protein-Bound Lipoic Acid

(A) Deficient lipoylation of PDHc and KGDHc E2 subunits in individuals with *LIPT2* and *LIPT1* mutations. Protein lipoylation was studied by western blot in triplicate with an anti-lipoic acid (Abcam cat# ab58724, RRID: AB_880635, 1:1,600) and anti-porin antibody (Abcam cat# ab14734, RRID: AB_443084, 1:1,000). In fibroblasts from individuals with *LIPT2* mutations, the levels of the expected lipoyl-E2 subunits of PDHc and α-KGDHc were strongly decreased, whereas they were undetectable in an individual with LIPT1 deficiency.

(B) Deficient protein lipoylation in fibroblasts of affected individuals. Immunofluorescence staining analysis by a confocal Leica TCS SP8 (Leica) under a 40× NA 1.3 oil immersion objective and acquired using LAS X software revealed decreased protein lipoylation in LIPT2-P1 and LIPT2-P2 fibroblasts (rabbit anti-lipoic acid: Abcam cat# ab58724, RRID: AB_880635, 1:1,000; mouse anti-porin: Abcam cat# ab14734, RRID: AB_443084, 1:400).

1,000 exome-sequencing projects performed in the Imagine Institute.

To determine whether lipoic acid metabolism was impaired in individuals with *LIPT2* mutations, we used an antibody that specifically recognizes lipoic acid bound to proteins as previously described[7] and anti-porin antibody. Anti-lipoate antibody detected strongly decreased levels of the expected lipoylated E2 subunits of α-oxoacid dehydrogenases in fibroblasts of individuals P1 and P2, whereas normal bands were seen in the control (Figure 3A). In fibroblasts of an individual with LIPT1 deficiency,[7] these bands were undetectable (Figure 3A). Moreover, immunofluorescence staining examined by a confocal microscopy showed absence of protein lipoylation in P1 and P2 fibroblasts (Figure 3B). In P1 fibroblasts, *LIPT2* mRNA expression analyzed by quantitative PCR in triplicate and normalized to the *β-actin* mRNA level and protein levels analyzed by western blot in triplicate were normal, suggesting that the two mutations might not affect mRNA or protein stability (Figure 4A). In P2 fibroblasts, *LIPT2* mRNA was not decreased compared to control, but the variant c.314T>G was less abundant in Sanger sequencing results (Figure S4). Moreover, we examined LIPT2 localization using confocal microscopy in P1 skin fibroblasts (Figure 4B). Colocalization studies between the mitochondrial cytochrome *c* and LIPT2 showed a positive Pearson coefficient at 0.267 ± 0.014 for the affected individual and 0.241 ± 0.032 for the control, which demonstrated a colocalization between LIPT2 and cytochrome *c*. Cell surface colocalization was 11.7% ± 3.12% for P1 and 10.7% ± 2.37% for the control. Altogether, these results confirm the location of LIPT2 in mitochondria. To assess consequences of LIPT2 deficiency on mitochondria function, we measured oxygen consumption rate (OCR) in fibroblasts from healthy individuals and individuals with LIPT1[7] or LIPT2 deficiency using the XF Cell Mito Stress Test Kit and XFe96 analyzer (Seahorse Bioscience, Agilent Technologies) following the manufacturer's recommendations.[23] As shown in Figure 2, basal oxygen consumption rates did not differ significantly between different control and affected individuals' fibroblasts. However, when cells were challenged with a mitochondrial uncoupler (FCCP), significant differences in OCR in control and affected individuals' cells were revealed. As demonstrated by analyses presented on Figure 2, fibroblasts from healthy individuals had significantly higher maximal respiratory capacity than fibroblasts from individuals with either LIPT1 or LIPT2 deficiency. These observations in primary cells from affected individuals strongly suggest respiratory capacity failure downstream of mutated *LIPT1* or *LIPT2*. Finally, to demonstrate that *LIPT2* mutations are disease causing, P1 and P2 fibroblasts were transfected with a plasmid coding wild-type LIPT2-GFP. Immunostaining of protein-bound lipoic acid showed that expression of wild-type LIPT2 increased protein lipoylation in fibroblasts of P1 and P2 (Figure 5), suggesting that *LIPT2* mutations are responsible for defect of protein lipoylation in fibroblasts of affected individuals.

Wild-type and *Δlip2* strains, deleted for *LIP2*[29] (the gene orthologous to human *LIPT2*[4]), were grown on glucose (YPD) and glycerol (YPG) (non-fermentable carbon source) medium for 4 days at 28°C. A clear growth defect was observed for *Δlip2* cells on the respiratory glycerol medium (Figure S5A). Lipoic acid (2 ng/mL, 5 ng/mL, and 10 ng/mL) was added to the non-fermentable growth medium to test its potential therapeutic effects, but it did not improve *Δlip2* growth (Figure S5A). Accordingly, fibroblasts cultures of P1 and a control were supplemented

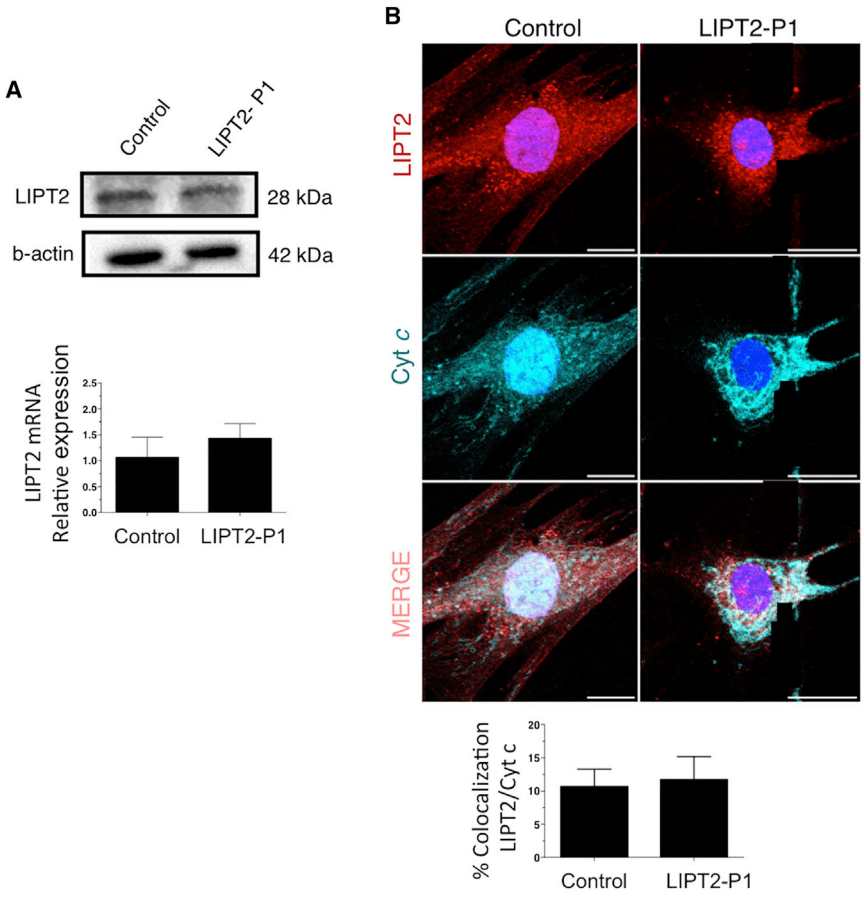

Figure 4. Immunoblot Analysis, mRNA Expression, and Immunofluorescence of LIPT2 in Fibroblasts

(A) Fibroblasts of LIPT2-P1 and control contain similar amount of LIPT2 protein and mRNA. LIPT2 protein level was studied three times (anti-LIPT2 antibody: ab173981 Abcam, 1:500; anti-β-actin: Sigma-Aldrich cat# A5441, RRID: AB_476744, 1:10,000). *LIPT2* mRNA expression was analyzed by quantitative PCR and normalized to the *β-actin* mRNA level (ABI PRISM 7300 Sequence Detection System instrument; TaqMan Universal PCR Master Mix from Applied Biosystem). Data are presented as mean ± SD of triplicates. For studies in LIPT2-P1 fibroblasts, primer sequences are: forward primer *LIPT2*: 5′-CGT GGT TTG AGC ACA TCG-3′; reverse primer *LIPT2*: 5′-AAG GCC ACA AGG AAA GGT G-3′.

(B) Fibroblasts from LIPT2-P1 and control exhibited colocalization of cytochrome *c* and LIPT2. Rabbit anti-LIPT2 (Novus Biological, Immunifluorescence [IF] 1:100) and mouse anti-cytochrome *c* (BD PharMingen; IF: 1:100) were used to study LIPT2 localization. The amount of co-localization between two channels was quantified using thresholded Pearson's correlation coefficients with JACoP[28] plugin from NIH FIJI software (v.1.51a). To quantify mitochondrial areas and the amount of co-localization at peripheral sites, threshold Pearson's coefficients were calculated in three randomly chosen 100 pixel × 100 pixel squares in the cell periphery. For averaged line scans, line profiles were calculated as the mean fluorescence intensity averaged over 100 pixels. Maximum intensity projections were calculated from z stacks with 500 nm spacing between slices covering the whole cell. For analysis of immunocytochemistry experiments, a minimum of three independent experiments was performed and statistically significant estimates for each sample were obtained by choosing an appropriate sample size, correlating to 15–40 images per condition per experiment for microscopy-based quantifications. Cells were chosen arbitrarily according to the fluorescent signal in a separate channel, which was not used for quantification. Data are presented as mean ± standard deviation. Statistical tests were performed using a two-tailed, unpaired t test, without excluding samples from statistical analysis. Images were computed using the plugin FigureJ (Jerome Muitterer and Edda Zinck; v.1.10b) on FIJI software.

with lipoic acid (Sigma) to a final concentration of 100 μM for 3 weeks. Biochemical investigations were performed before and after 3 weeks of supplementation. As in LIPT1 individual's fibroblasts,[7] this treatment only moderately increased PDHc (276–279 pmol/min/mg of protein) and αKGDHc (1.4 ± 0.3 to 3.5 ± 0.7 nmol/min/mg of protein) activities and did not modify metabolic flux nor PDHc and αKGDHc E2 subunit lipoylation (Figures S5B and S5C).

Consistent with previous reports on *LIAS* and *LIPT1* mutations,[7,30] we provide evidence that impaired attachment of lipoate on mitochondrial proteins in LIPT2-deficient individuals accounts for impaired activities of PDHc and α-KGDHc along with altered branched-chain amino acid catabolism. While lactate levels at the beginning of the investigations and brain MRI were indicative of perturbed energy metabolism, hyperlactatemia was inconstant during follow-up and pyruvate levels were not increased either in plasma or CSF in P1, thus not suggestive of PDHc deficiency prior to in vitro studies. This finding adds to the evidence that standard biochemical tests may not be fully informative to detect related energetic disorders that involve PDHc deficiency. We propose that systematic screening of PDHc or pyruvate oxidation by polarography should be performed in unresolved cases of suspected energetic diseases, or alternatively and more efficiently, that all the genes of this new pathway should be included in an NGS-based screening approach; then, enzymatic analysis can confirm the supposed deficit. Other key enzymatic complexes with similar structure and LA dependence, such as α-KGDHc, BCKDHc, and probably GCS, can be affected. Surprisingly, branched-chain amino acids concentrations were low in plasma of P1 at presentation and during follow-up despite the decrease of leucine catabolism revealed by $^{13}C_6$ leucine loading test. Other essential amino acids were in the lower range of normal value. Low branched-chain amino acid concentrations were also observed in P2 and in previously reported lipoic acid synthesis defects with either LIPT1[7] or LIAS[6] deficiency. On the other hand, it is important to note that a large proportion of individuals with related disorders such as

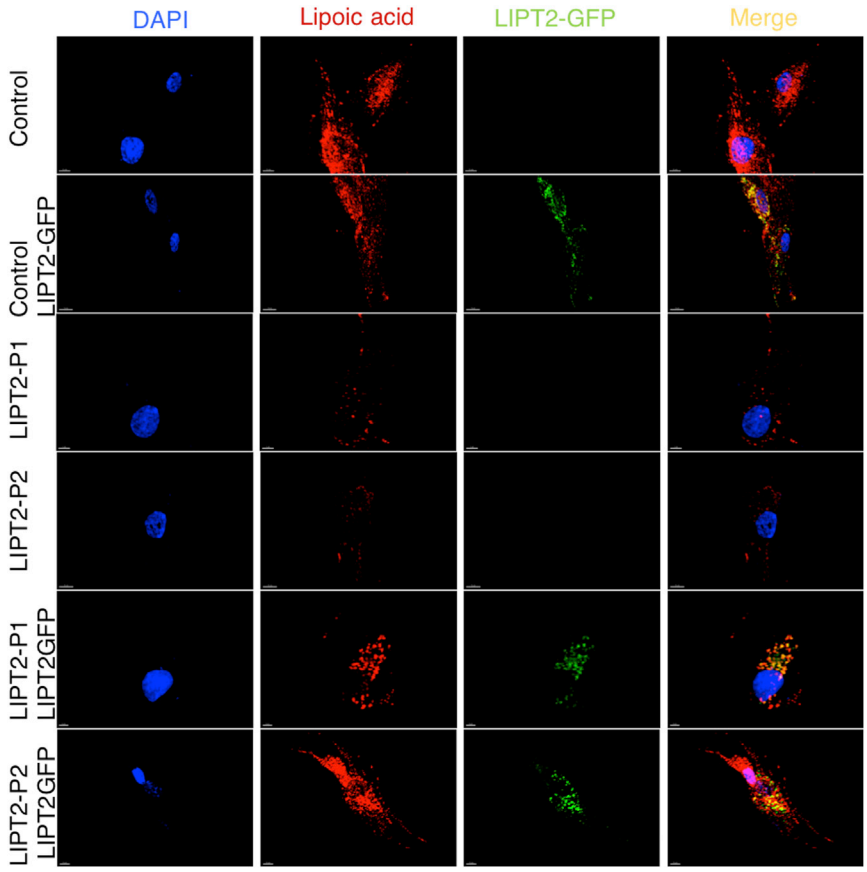

Figure 5. Rescue of Protein Lipoylation in Affected Individuals with LIPT2 Deficiency

Fibroblasts from affected individuals were transfected with wild-type *LIPT2*. Immunostaining analysis of protein-bound lipoic acid showed increase of protein lipoylation after transfection. The following antibodies and reagents were used: rabbit anti-LIPT2 (Novus Biological, ImmunoFluorescence [IF]: 1:100), rabbit anti-lipoic acid (Abcam cat# ab58724, RRID: AB_880635; 1:1,000), and DAPI 300 nM in PBS (D1306, Molecular Probes).

E3 subunit[31] and NFU1 deficiency[13] have shown only transient or intermittent biochemical abnormalities. Therefore, there is a large heterogeneity of clinical and biochemical spectrum in these diseases. Compared to other essential amino acids, plasma levels of branched-chain amino acids are known to be most sensitive to nutritional deprivation, thus raising the possibility that feeding difficulties may mask the expected increase of branched-chain amino acids. In this context, $^{13}C_6$ leucine loading test is particularly interesting to reveal BCKDHc defects when they are not obvious on plasma amino acid profiling. During follow-up, glutamate and glutamine concentrations were increased, ammonemia being normal. This is probably the consequence of increased catabolism due to denutrition and reflects α-KGDHc deficiency too.

In P1 and P2, blood glycine concentrations were increased. In P1, this increase was mild at presentation and more marked during follow-up. Blood glycine concentrations were similar or higher than those observed in some cases of NFU1 deficiency with small amounts of normal *NFU1* transcript and strongly decreased but detectable E2 subunit lipoylation.[14] Conversely, because LIPT1 acts downstream of GCS H lipoylation, glycine was normal in individuals with LIPT1 deficiency.[7,8] Indeed, the current model of the de novo pathway states that LIPT2 and LIAS are involved in the lipoylation of GCS H protein, whereas LIPT1 is responsible for the transfer of lipoyl moiety from lipoyl GCS H protein to the BCKDHc, PDHc, and α-KGDHc E2 subunits. Moreover, Schonauer et al. showed that, in a Δ*lip2* yeast strain, Gcv3 (the GCS H ortholog) was not lipoylated.[4]

Defects in the ISC assembly involve LA de novo biosynthesis because LIAS is an ISC-dependent enzyme, but they include multiple additional dysfunctions that involve succinate dehydrogenase and aconitase 2, two proteins from the tricarboxylic acid cycle, as well as the respiratory chain complexes I–III,[16,32] thus contrasting with normal activities in our individuals with *LIPT2* mutations or those with LIAS and LIPT1 deficiency. This may explain why in individuals with [Fe-S] cluster pathway deficiencies, both neurological and non-neurological multisystem symptoms were reported.[9,10,18] In contrast, the clinical picture of LIPT1, LIAS, and LIPT2-related individuals was mostly limited to the brain, thus similar to primary PDHc deficiencies. The much greater severity of the neurological features in the LA disorders relative to primary PDHc deficiencies might partly result from the additional α-KGDHc enzyme defect. LIPT2-P1 had less pronounced biochemical markers of energetic deficiency than individuals harboring mutations in *LIPT1* and other genes, yet brain abnormalities were comparable. The white matter is frequently impaired in LA and ISC defects, including leukoencephalopathy with cysts in individuals harboring mutations in *LIPT2*, and white matter abnormalities and delayed myelination in *LIPT1*-related individuals.[7,8] We propose that the diagnostic work-up of an encephalopathy associated with white matter abnormalities and hyperglycinaemia (the latter missing only in individuals with *LIPT1* mutations) should include LA mitochondrial synthesis defects, even in the absence of hyperlactatemia in the basal state.

Finally, a major challenge for this new and severe enzyme cofactor disease is therapy. Since PDHc was found decreased in P3, a ketogenic diet was tried in P2, the younger brother of P3. Lactic acidosis improved under this treatment while his clinical condition worsened and he lost weight. This is in accordance with our negative

experience with ketogenic diet in an individual with NFU1 deficiency (unpublished results). Indeed, although ketogenic diet bypasses PDHc, it cannot circumvent α-KGDHc acting downstream. While lipoic acid supplementation partly rescued the growth of yeasts deficient in the *LIPT1* ortholog,[7] it did not restore Δ*lip2* yeast strain growth in agreement with previous studies.[29] In P1-derived fibroblasts, functional studies did not show improvement in the presence of LA, and the clinical condition of the affected individual P1 remained unchanged under LA supplementation, as already shown in other defects of the lipoylation pathway in yeast, mouse, and human cells.[4,6,7,9,16,18] Oral LA supplementation was also ineffective in two cases of NFU1 deficiency,[13,15] supporting the proposal that in contrast to bacteria, eukaryotic cells cannot use exogenously supplied LA (salvage pathway) and they depend exclusively on de novo intramitochondrial synthesis.[33,34] Other mechanisms, such as partial redundancy between LIPT1 and LIPT2 operating either upstream of LIAS and/or in the usage of free AMP-LA as a substrate, can also be excluded.

In conclusion, we reported here pathogenic *LIPT2* mutations, and we showed that these mutations altered lipoate binding in the E2 subunit of α-oxoacid dehydrogenases. The clinical phenotype of LIPT2 deficiency is similar to other lipoic acid synthesis defects, especially LIAS and LIPT1 deficiencies, characterized by an impressive degree of early-onset encephalopathy.

Supplemental Data

Supplemental Data include one Supplemental Note (Case Reports), five tables, and five figures and can be found with this article online at http://dx.doi.org/10.1016/j.ajhg.2017.07.001.

Acknowledgments

We thank Mohammed Zarhrate for his technical support. This work was supported by Fondation Lejeune (grant 2014), Fondation Bettencourt 2012, AFM 2012-2014 (number 15947), ANR 2013-2016 (ANR-13-BSV1-0020), Association contre les Maladies Mitochondriales (AMMI), Association Nos Anges, and Association Hyperinsulinisme. We are indebted to the Necker Cell Imaging Platform for helpful discussions about cellular analyses. T.B.H. work was supported by the German Federal Ministry of Education and Research (BMBF) within the framework of the e:Med research and funding concept (grant #FKZ 01ZX1405C). Supported by the E-Rare project GENOMIT (01GM1207 and 01GM1603 to H.P., O1GML 1207 to A.R.) and Austrian Science Fonds (FWF) (I 2741-B26 to J.A.M.).

Received: March 28, 2017
Accepted: July 5, 2017
Published: July 27, 2017

Web Resources

Ali2D, https://toolkit.tuebingen.mpg.de
Clustal Omega, http://www.ebi.ac.uk/Tools/msa/clustalo/
GenBank, http://www.ncbi.nlm.nih.gov/genbank/
gnomAD Browser, http://gnomad.broadinstitute.org/
HUGO Gene Nomenclature Committee, http://www.genenames.org/
OMIM, http://www.omim.org/
RRID, https://scicrunch.org/resources

References

1. Fujiwara, K., Okamura-Ikeda, K., and Motokawa, Y. (1994). Purification and characterization of lipoyl-AMP:N epsilon-lysine lipoyltransferase from bovine liver mitochondria. J. Biol. Chem. *269*, 16605–16609.
2. Fujiwara, K., Suzuki, M., Okumachi, Y., Okamura-Ikeda, K., Fujiwara, T., Takahashi, E., and Motokawa, Y. (1999). Molecular cloning, structural characterization and chromosomal localization of human lipoyltransferase gene. Eur. J. Biochem. *260*, 761–767.
3. Booker, S.J. (2004). Unraveling the pathway of lipoic acid biosynthesis. Chem. Biol. *11*, 10–12.
4. Schonauer, M.S., Kastaniotis, A.J., Kursu, V.A., Hiltunen, J.K., and Dieckmann, C.L. (2009). Lipoic acid synthesis and attachment in yeast mitochondria. J. Biol. Chem. *284*, 23234–23242.
5. Hiltunen, J.K., Autio, K.J., Schonauer, M.S., Kursu, V.A., Dieckmann, C.L., and Kastaniotis, A.J. (2010). Mitochondrial fatty acid synthesis and respiration. Biochim. Biophys. Acta *1797*, 1195–1202.
6. Mayr, J.A., Zimmermann, F.A., Fauth, C., Bergheim, C., Meierhofer, D., Radmayr, D., Zschocke, J., Koch, J., and Sperl, W. (2011). Lipoic acid synthetase deficiency causes neonatal-onset epilepsy, defective mitochondrial energy metabolism, and glycine elevation. Am. J. Hum. Genet. *89*, 792–797.
7. Soreze, Y., Boutron, A., Habarou, F., Barnerias, C., Nonnenmacher, L., Delpech, H., Mamoune, A., Chrétien, D., Hubert, L., Bole-Feysot, C., et al. (2013). Mutations in human lipoyltransferase gene LIPT1 cause a Leigh disease with secondary deficiency for pyruvate and alpha-ketoglutarate dehydrogenase. Orphanet J. Rare Dis. *8*, 192.
8. Tort, F., Ferrer-Cortès, X., Thió, M., Navarro-Sastre, A., Matalonga, L., Quintana, E., Bujan, N., Arias, A., García-Villoria, J., Acquaviva, C., et al. (2014). Mutations in the lipoyltransferase LIPT1 gene cause a fatal disease associated with a specific lipoylation defect of the 2-ketoacid dehydrogenase complexes. Hum. Mol. Genet. *23*, 1907–1915.
9. Navarro-Sastre, A., Tort, F., Stehling, O., Uzarska, M.A., Arranz, J.A., Del Toro, M., Labayru, M.T., Landa, J., Font, A., Garcia-Villoria, J., et al. (2011). A fatal mitochondrial disease is associated with defective NFU1 function in the maturation of a subset of mitochondrial Fe-S proteins. Am. J. Hum. Genet. *89*, 656–667.
10. Haack, T.B., Rolinski, B., Haberberger, B., Zimmermann, F., Schum, J., Strecker, V., Graf, E., Athing, U., Hoppen, T., Wittig, I., et al. (2013). Homozygous missense mutation in BOLA3 causes multiple mitochondrial dysfunctions syndrome in two siblings. J. Inherit. Metab. Dis. *36*, 55–62.
11. Ajit Bolar, N., Vanlander, A.V., Wilbrecht, C., Van der Aa, N., Smet, J., De Paepe, B., Vandeweyer, G., Kooy, F., Eyskens, F., De Latter, E., et al. (2013). Mutation of the iron-sulfur cluster assembly gene IBA57 causes severe myopathy and encephalopathy. Hum. Mol. Genet. *22*, 2590–2602.
12. Lim, S.C., Friemel, M., Marum, J.E., Tucker, E.J., Bruno, D.L., Riley, L.G., Christodoulou, J., Kirk, E.P., Boneh, A., DeGennaro,

C.M., et al. (2013). Mutations in LYRM4, encoding iron-sulfur cluster biogenesis factor ISD11, cause deficiency of multiple respiratory chain complexes. Hum. Mol. Genet. *22*, 4460–4473.
13. Nizon, M., Boutron, A., Boddaert, N., Slama, A., Delpech, H., Sardet, C., Brassier, A., Habarou, F., Delahodde, A., Correia, I., et al. (2014). Leukoencephalopathy with cysts and hyperglycinemia may result from NFU1 deficiency. Mitochondrion *15*, 59–64.
14. Ferrer-Cortès, X., Narbona, J., Bujan, N., Matalonga, L., Del Toro, M., Arranz, J.A., Riudor, E., Garcia-Cazorla, A., Jou, C., O'Callaghan, M., et al. (2016). A leaky splicing mutation in NFU1 is associated with a particular biochemical phenotype. Consequences for the diagnosis. Mitochondrion *26*, 72–80.
15. Tonduti, D., Dorboz, I., Imbard, A., Slama, A., Boutron, A., Pichard, S., Elmaleh, M., Vallée, L., Benoist, J.F., Ogier, H., and Boespflug-Tanguy, O. (2015). New spastic paraplegia phenotype associated to mutation of NFU1. Orphanet J. Rare Dis. *10*, 13.
16. Rouault, T.A., and Tong, W.H. (2008). Iron-sulfur cluster biogenesis and human disease. Trends Genet. *24*, 398–407.
17. Booker, S.J., Cicchillo, R.M., and Grove, T.L. (2007). Self-sacrifice in radical S-adenosylmethionine proteins. Curr. Opin. Chem. Biol. *11*, 543–552.
18. Cameron, J.M., Janer, A., Levandovskiy, V., Mackay, N., Rouault, T.A., Tong, W.H., Ogilvie, I., Shoubridge, E.A., and Robinson, B.H. (2011). Mutations in iron-sulfur cluster scaffold genes NFU1 and BOLA3 cause a fatal deficiency of multiple respiratory chain and 2-oxoacid dehydrogenase enzymes. Am. J. Hum. Genet. *89*, 486–495.
19. Kishita, Y., Pajak, A., Bolar, N.A., Marobbio, C.M., Maffezzini, C., Miniero, D.V., Monné, M., Kohda, M., Stranneheim, H., Murayama, K., et al. (2015). Intra-mitochondrial methylation deficiency due to mutations in SLC25A26. Am. J. Hum. Genet. *97*, 761–768.
20. Rustin, P., Chrétien, D., Bourgeron, T., Gérard, B., Rötig, A., Saudubray, J.M., and Munnich, A. (1994). Biochemical and molecular investigations in respiratory chain deficiencies. Clin. Chim. Acta *228*, 35–51.
21. Imbard, A., Boutron, A., Vequaud, C., Zater, M., de Lonlay, P., de Baulny, H.O., Barnerias, C., Miné, M., Marsac, C., Saudubray, J.M., and Brivet, M. (2011). Molecular characterization of 82 patients with pyruvate dehydrogenase complex deficiency. Structural implications of novel amino acid substitutions in E1 protein. Mol. Genet. Metab. *104*, 507–516.
22. Brivet, M., Garcia-Cazorla, A., Lyonnet, S., Dumez, Y., Nassogne, M.C., Slama, A., Boutron, A., Touati, G., Legrand, A., and Saudubray, J.M. (2003). Impaired mitochondrial pyruvate importation in a patient and a fetus at risk. Mol. Genet. Metab. *78*, 186–192.
23. Vergnes, L., Chin, R., Young, S.G., and Reue, K. (2011). Heart-type fatty acid-binding protein is essential for efficient brown adipose tissue fatty acid oxidation and cold tolerance. J. Biol. Chem. *286*, 380–390.
24. Yoshida, I., Sweetman, L., and Nyhan, W.L. (1986). Metabolism of branched-chain amino acids in fibroblasts from patients with maple syrup urine disease and other abnormalities of branched-chain ketoacid dehydrogenase activity. Pediatr. Res. *20*, 169–174.
25. Kremer, L.S., Danhauser, K., Herebian, D., Petkovic Ramadža, D., Piekutowska-Abramczuk, D., Seibt, A., Müller-Felber, W., Haack, T.B., Płoski, R., Lohmeier, K., et al. (2016). NAXE mutations disrupt the cellular NAD(P)HX repair system and cause a lethal neurometabolic disorder of early childhood. Am. J. Hum. Genet. *99*, 894–902.
26. Li, H., and Durbin, R. (2009). Fast and accurate short read alignment with Burrows-Wheeler transform. Bioinformatics *25*, 1754–1760.
27. Li, H., Handsaker, B., Wysoker, A., Fennell, T., Ruan, J., Homer, N., Marth, G., Abecasis, G., Durbin, R.; and 1000 Genome Project Data Processing Subgroup (2009). The Sequence Alignment/Map format and SAMtools. Bioinformatics *25*, 2078–2079.
28. Bolte, S., and Cordelières, F.P. (2006). A guided tour into subcellular colocalization analysis in light microscopy. J. Microsc. *224*, 213–232.
29. Marvin, M.E., Williams, P.H., and Cashmore, A.M. (2001). The isolation and characterisation of a *Saccharomyces cerevisiae* gene (LIP2) involved in the attachment of lipoic acid groups to mitochondrial enzymes. FEMS Microbiol. Lett. *199*, 131–136.
30. Mayr, J.A., Feichtinger, R.G., Tort, F., Ribes, A., and Sperl, W. (2014). Lipoic acid biosynthesis defects. J. Inherit. Metab. Dis. *37*, 553–563.
31. Brassier, A., Ottolenghi, C., Boutron, A., Bertrand, A.M., Valmary-Degano, S., Cervoni, J.P., Chrétien, D., Arnoux, J.B., Hubert, L., Rabier, D., et al. (2013). Dihydrolipoamide dehydrogenase deficiency: a still overlooked cause of recurrent acute liver failure and Reye-like syndrome. Mol. Genet. Metab. *109*, 28–32.
32. Rouault, T.A. (2012). Biogenesis of iron-sulfur clusters in mammalian cells: new insights and relevance to human disease. Dis. Model. Mech. *5*, 155–164.
33. Sulo, P., and Martin, N.C. (1993). Isolation and characterization of LIP5. A lipoate biosynthetic locus of *Saccharomyces cerevisiae*. J. Biol. Chem. *268*, 17634–17639.
34. Morris, T.W., Reed, K.E., and Cronan, J.E., Jr. (1995). Lipoic acid metabolism in Escherichia coli: the lplA and lipB genes define redundant pathways for ligation of lipoyl groups to apoprotein. J. Bacteriol. *177*, 1–10.

The American Journal of Human Genetics, Volume *101*

Supplemental Data

Biallelic Mutations in *LIPT2* Cause a Mitochondrial Lipoylation Defect Associated with Severe Neonatal Encephalopathy

Florence Habarou, Yamina Hamel, Tobias B. Haack, René G. Feichtinger, Elise Lebigot, Iris Marquardt, Kanetee Busiah, Cécile Laroche, Marine Madrange, Coraline Grisel, Clément Pontoizeau, Monika Eisermann, Audrey Boutron, Dominique Chrétien, Bernadette Chadefaux-Vekemans, Robert Barouki, Christine Bole-Feysot, Patrick Nitschke, Nicolas Goudin, Nathalie Boddaert, Ivan Nemazanyy, Agnès Delahodde, Stefan Kölker, Richard J. Rodenburg, G. Christoph Korenke, Thomas Meitinger, Tim M. Strom, Holger Prokisch, Agnes Rotig, Chris Ottolenghi, Johannes A. Mayr, and Pascale de Lonlay

Supplemental Note: Case Reports

Individual 1 (P1), a boy, was the first child of non-consanguineous parents of French (mother) and Ivory Coast (father) origin. He was born after an uneventful pregnancy and spontaneous delivery at term with normal birth parameters (body weight 3,750 g, length 51 cm, head circumference 35 cm). Apgar scores were 9/10/10. From birth on, he presented with truncal hypotonia, spastic tetraparesis, and dystonia. Brain MRI showed marked supra-tentorial cortical atrophy with ventricular dilatation as well as bi-frontal white matter abnormalities and delayed myelination (Figure 1A middle). MRS spectroscopy with a long TE (144) showed a lactate peak (Figure 1B). This clinical and radiological presentation led us to suspect a mitochondrial disease. At age 2.5 years, the affected individual was bed- and wheelchair-bound with no head control. He could neither sit unaided nor speak or understand simple orders. He was otherwise fully conscious and alert, and he could smile at times and follow with his eyes. His weight was -2.5 SD, his length was at the median, and his head circumference (HC) was -4 SD. Major swallowing difficulties led to gastrostomy. At the age of 3 years, he developed complex epilepsy treated by oxcarbazepine (Trileptal®), clobazam (Urbanyl®), and topiramate (Epitomax®). Electroencephalography at the age of 7 years showed in the awake state, an absence of occipital alpha rhythm, polyrhythmic background activity with diffuse alpha, theta and rare delta rhythms, multifocal spikes and sharp waves, sometimes in bursts or rhythmic sequences, with right posterior predominance (Figure S3A). Cardiac ultrasonography, audiological and ophthalmological examination were normal. At the age of 7 years and 9 months, the ventricular dilatation and sub-tentorial cortical atrophy were increased. No episodes of metabolic decompensation have been documented.

Affected individual 2 (P2) and 3 (P3) are born from healthy parents of German origin. P2, a boy, was born at the 39th week of gestation by caesarean section due to a gestational diabetes of the mother (BMI 40). Apgar scores were 9/10/10 and birth parameters within normal range (body weight 3,180 g, length 51 cm, head circumference 38 cm). Lactate concentration was 3.7 mmol/L initially and increased to values between 8 and 10, in a single measurement up to 111 mmol/L (N<1.8 mmol/L). The child showed severe muscular hypotonia. Newborn reflexes could only partially be induced. Brain sonography showed mildly enlarged lateral ventricles at the third day of life (data not shown), which was confirmed by brain MRI performed at 4 weeks showing also periventricular cystic changes. According to

sonographic investigations these changes were progressive. EEG performed at the age of 7 days showed neither awake-sleep differentiation nor physiological grapho-elements, background activity was persistently low-voltaged with amplitudes under 15 μV (Figure S3B). Myoclonic twitches were observed during sleep, however without EEG correlate. Otoacoustic emission was pathologic on both sides. Newborn screening did not reveal any abnormalities. A ketogenic diet was started, which resulted in a decrease of lactate concentrations but also lead to a weight loss and worsening of his condition. The child died at the age of 2 months.

Affected individual 3 (P3), the older sister of P2, was born spontaneously at 34 weeks of gestation. Apgar scores were 5/5/9, birth weight 2,400 g. She showed problems in respiratory adaptation and was ventilated by continuous positive airway pressure (CPAP) for 3 hours. Severe lactic acidosis up to 17 mmol/L was observed and further on respiratory decompensation and signs suspicious of epilepsy treated by phenobarbital. EEG at the (chronological) age of 3 weeks was abnormal lacking physiological grapho-elements and sleep-wake differentiation, showing reduced amplitudes (below 20 μV), however on phenobarbital treatment. There was no pattern typical for epilepsy. EEG at the age of 5 months was still pathological without physiological elements, however showing a richer background activity. At the age of 6 months multifocal spikes and sharp waves were noticed (Figure S3 C, D and E). Brain sonography at one week was suspicious for intraventricular hemorrhage with hypoechogenic areas adjacent to the 3rd and 4th ventricle (data not shown). At the age of 3 weeks micro- and macrocystic changes of the parietal brain parenchyma on both sides were noted. Brain MRI showed enlarged lateral ventricles and formation of cysts in the cortex and white matter of the whole cerebral structures. Furthermore, gyration of the cerebral hemispheres was decreased (Figure 1A bottom). Echocardiography showed a mild septum hypertrophy but normal ventricular function. The child died at the age of 7 months.

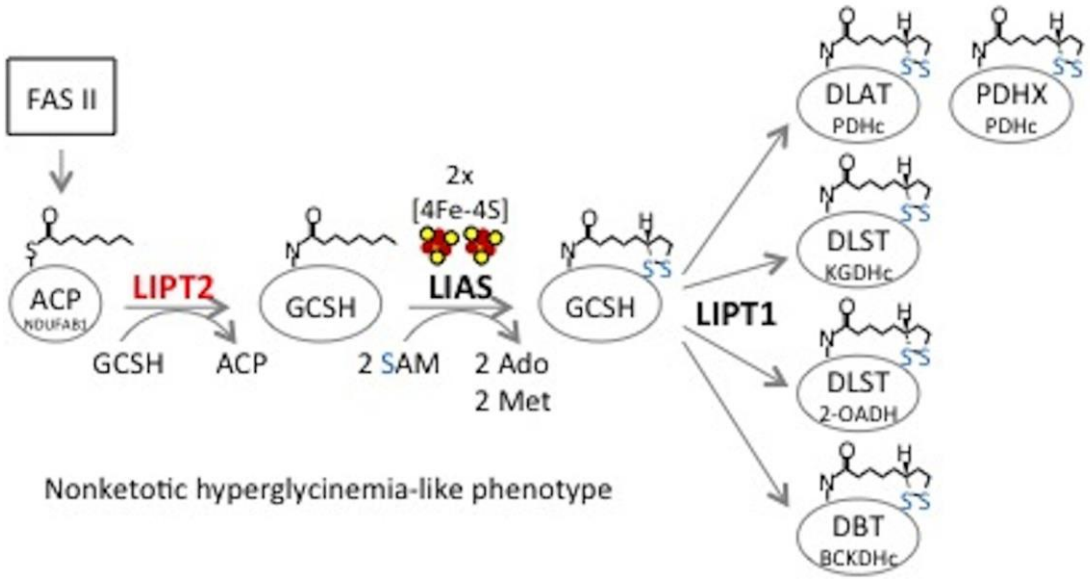

Figure S1. Synthesis of the lipoate cofactor in mitochondria.

Mitochondrial fatty acid synthesis (FAS II) forms octanoic acid bound to the mitochondrial acylcarrier protein (ACP) encoded by *NDUFAB1*. LIPT2 transfers the octanoic acid residue to the glycine cleavage H protein (GCSH). Lipoate is formed by the action of lipoic acid synthetase (LIAS), which uses S-adenosylmethionine (SAM) as a substrate and depends on two [4Fe-4S] iron-sulfur cluster cofactors. Finally LIPT1 transfers the lipoate residue from GCSH to E2 subunits of either pyruvate dehydrogenase complex (PDHc; pyruvate oxidation), α-oxoglutarate dehydrogenase complex (KGDHc; Krebs cycle), 2-oxoadipate dehydrogenase (2-OADH; lysine degradation), and branched-chain ketoacid dehydrogenase complex (BCKDHc; leucine, isoleucine, valine catabolism). Furthermore lipoate is transferred to the PDHX subunit of PDHc.

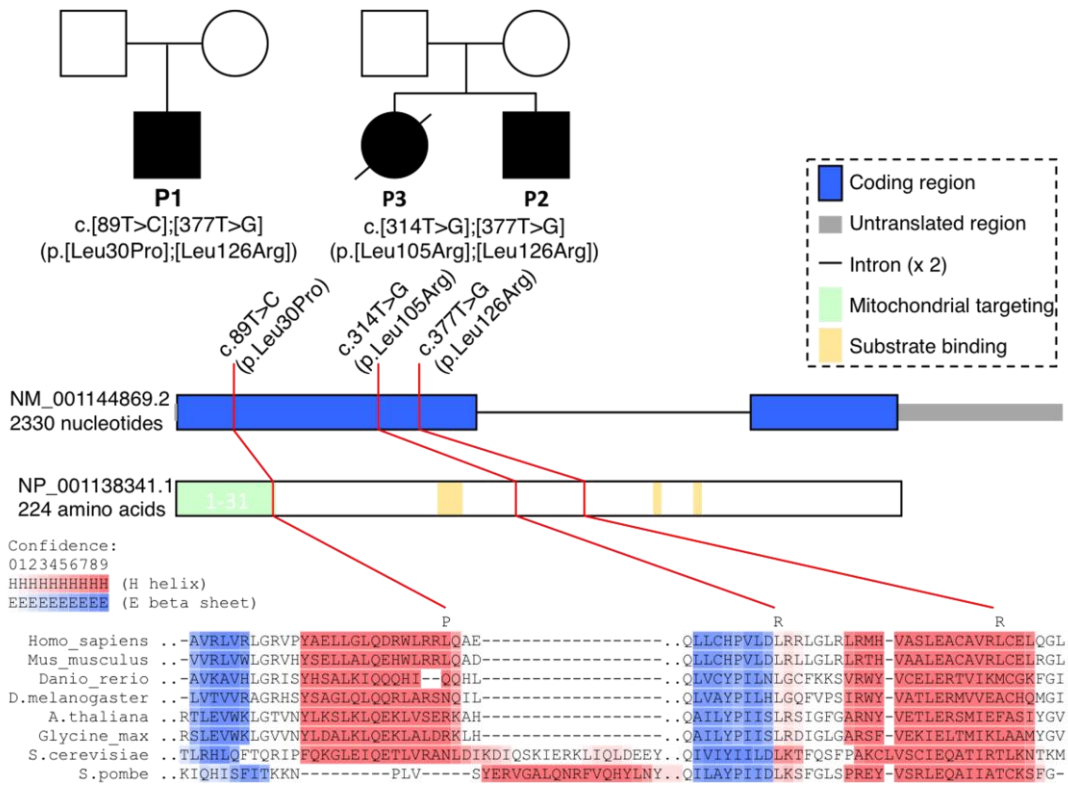

Figure S2. Pedigrees of affected individuals with LIPT2 deficiency and localization of mutations.

Three missense mutations have been identified showing different degree of phylogenetic conservation. Alignment was performed by ClustalOmega (http://www.ebi.ac.uk/Tools/msa/clustalo/). Secondary structure prediction was performed by Ali2D (https://toolkit.tuebingen.mpg.de/ali2d/)

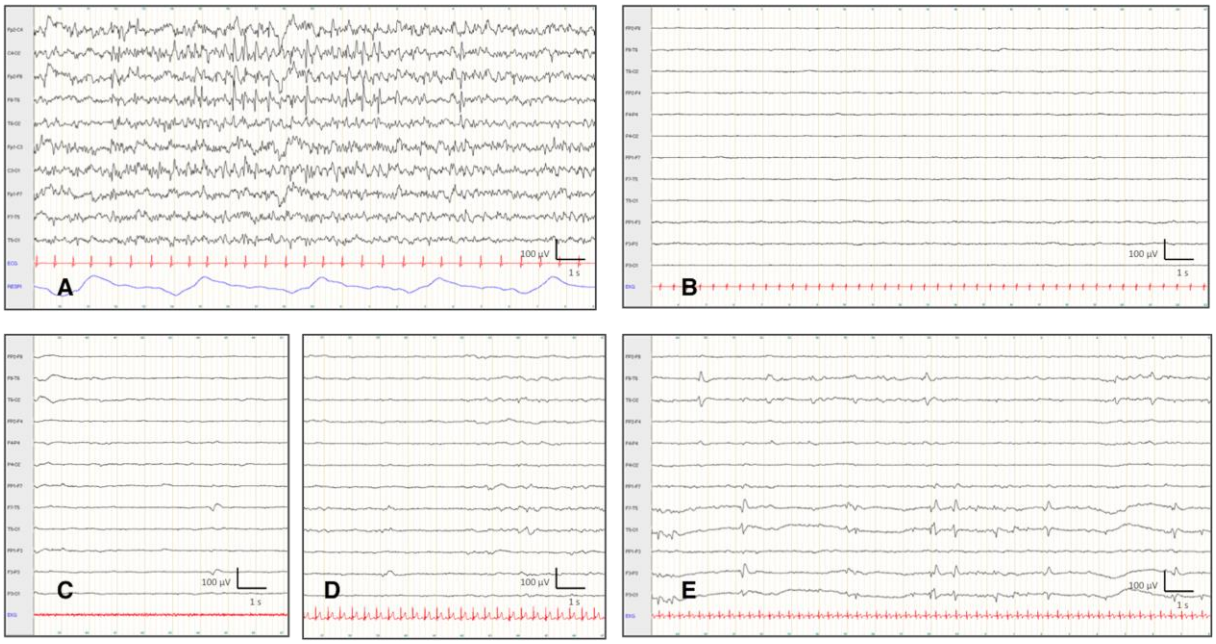

Figure S3: Electroencephalography in individuals with LIPT2 deficiency

A: P1 at the age of 7 years. Awake state. Polyrhythmic background activity with diffuse alpha, theta and rare delta rhythms, multifocal spikes and sharp waves, sometimes in bursts or rhythmic sequences, with right posterior predominance. **B: P2 at the age of 7 days.** Clinically quiet sleep. Background activity undifferentiated compared to awake state and active sleep, low-voltaged with amplitudes under 15 µV. **C: P3 at the age of 3 weeks (chronological age).** Clinically quiet sleep. Background activity undifferentiated compared to awake state and active sleep, low-voltaged with amplitudes under 20 µV. **D: P3 at the age of 5 months (chronological age).** Clinically sleep. Low-voltage activity, no physiological sleep figures. **E: P3 at the age of 6 months (chronological age).** Awake state. Low-voltage background activity, multifocal low amplitude spikes and sharp waves with left parieto-temporal predominance.

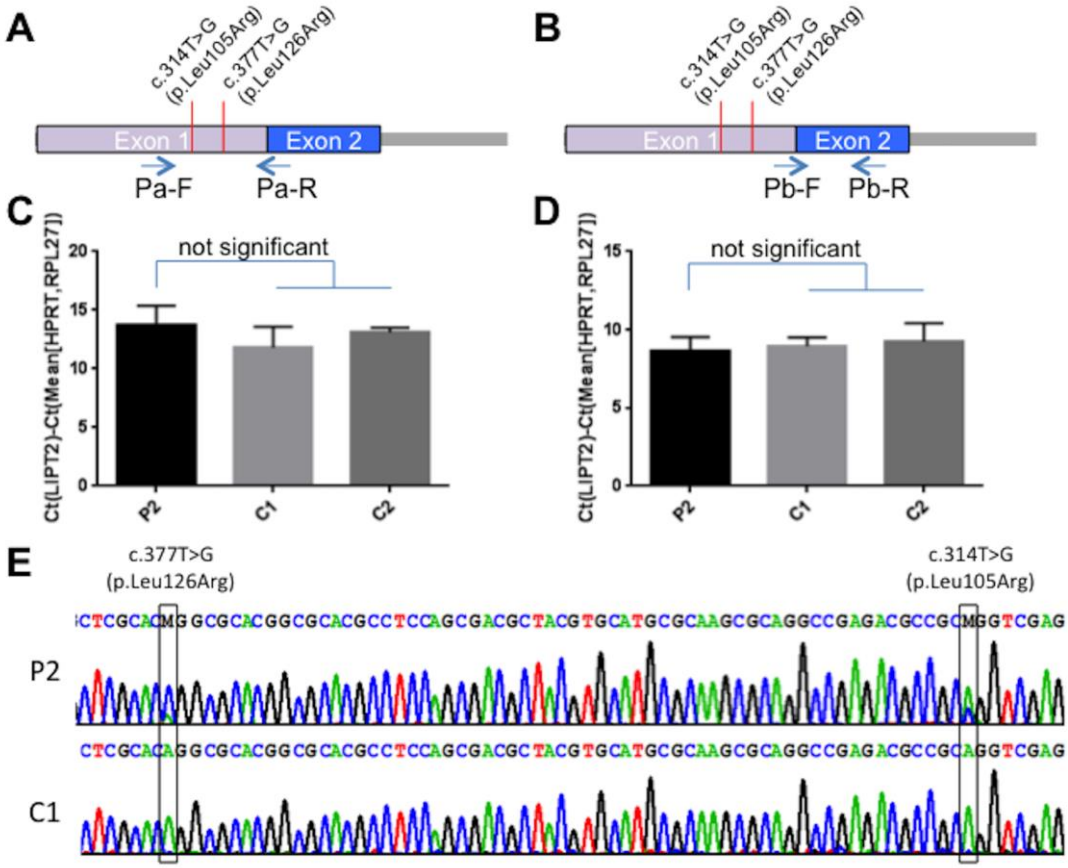

Figure S4. Expression analysis of *LIPT2* in fibroblasts of P2.

Quantitative real-time PCR of *LIPT2* cDNA was performed with the following set of primers: (A, C) Pa-F (forward), 5‘-GGCCTGGCCACCTTCCAC-3‘ and Pa-R (reverse), 5‘-CCACAGCGGACTCCGATC-3‘ as well as (B, D) Pb-F (forward), 5‘-TCTGCGCGATCGGAGTCC-3‘ and Pb-R (reverse), 5‘-GTGGCATTACTTCTTCCACGG-3‘. Each experiment was done in duplicate and was repeated once (4 data points for each measurement). Delta Ct (cycle threshold) values were calculated in relation to two housekeeping genes (*HPRT*, *RPL27*). No significant differences in expression of *LIPT2* between P2 and two controls (C1, C2) was found when analyzed by one-way ANOVA. The *LIPT2* PCR product (A) was analyzed by Sanger sequencing with the reverse primer (E) and revealed the presence of both variants c.377T>G (p.Leu126Arg) and c.314T>G (p.Leu105Arg), the latter in a bit lower amount.

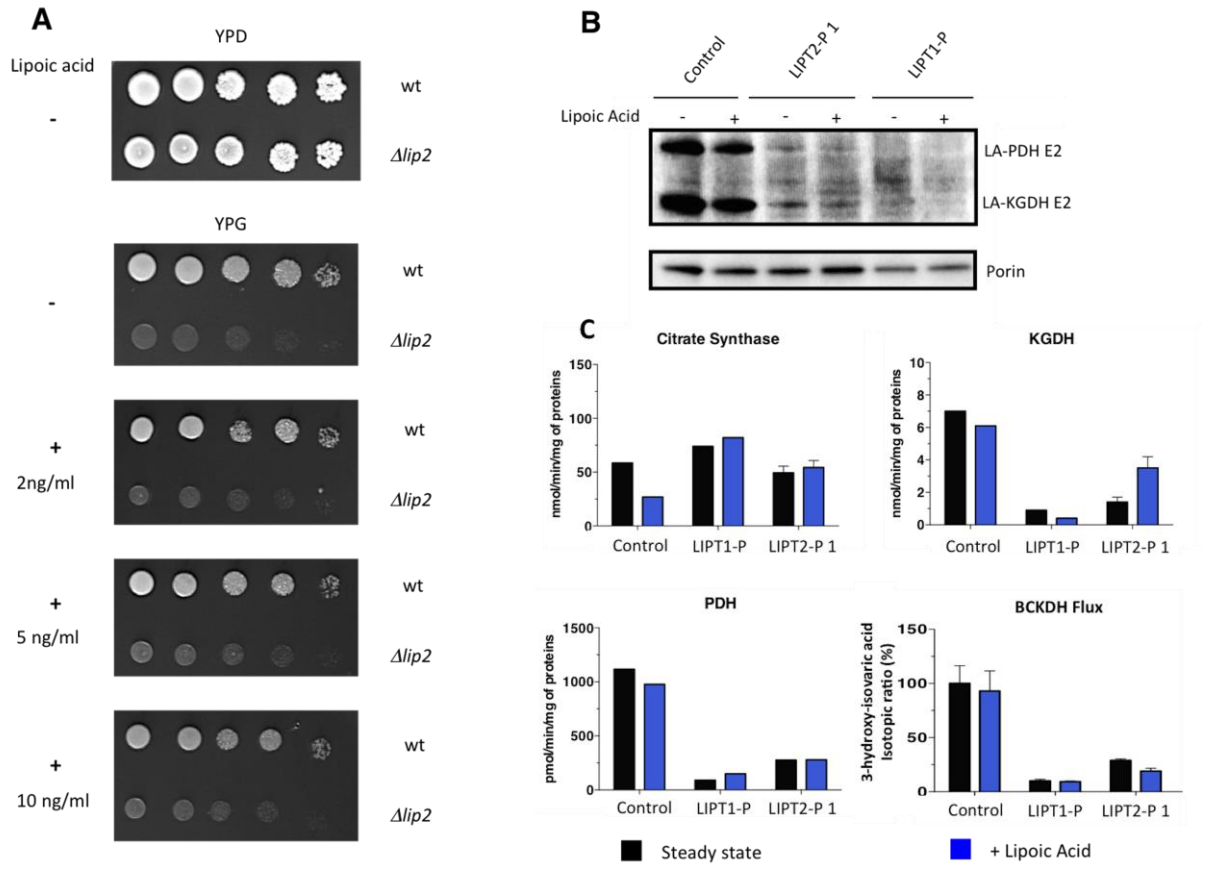

Figure S5: Effects of lipoic acid supplementation on Δ*lip2 (LIPT2 ortholog)*-deleted yeast strain and fibroblasts.

A: Δ*lip2*-deleted yeast strain failed to grow on YPG medium at 28 °C. Growth was not restored after lipoic acid supplementation. **B, C:** Fibroblasts were supplemented with 100 µM lipoic acid during three weeks. Lipoylation (studied in triplicates; anti-lipoic acid : ab58724, Abcam®, 1:1600; anti-porin antibody: ab14734, Abcam®, 1:1000) **(B)** and activities of α-oxoacid dehydrogenases (presented as means +/- SD) **(C)** were evaluated in basal conditions and after lipoic acid supplementation. They did not improve after treatment.

Table S1. Main clinical features in affected individuals.

	P1	P2	P3
Age of onset	Neonatal	Neonatal	Neonatal
Current age	10 years-old	Deceased at the age of 2 months, without any development	Deceased at the age of 7 months, without any development
Clinical and biological findings at presentation	Truncal hypotonia Spastic tetraparesis Dystonia Epilepsy Microcephaly Delayed psychomotor development Hyperlactatemia	Severe muscular hypotonia Lactic acidosis	Respiratory distress Lactic acidosis
MRI findings	Supra-tentorial cortical atrophy Ventricular dilatation Bifrontal white matter abnormalities Delayed myelination Progressive thalamus and putamen hyperintensities	Enlarged lateral ventricules Periventricular cystic changes	Enlarged lateral ventricules Cortical and white matter cystic abnormalities Decreased gyrification of the cerebral hemispheres

Table S2. Relevant plasma, urinary and CSF metabolites in LIPT2 affected individuals.

Reference intervals for each individual are provided as the ranges of the age-matched reference population. In P2, investigations were performed under ketogenic diet.

LIPT2-Individuals	**P1**					**P2**	**P3**
Age	**2.5 y**	**5 y**		**8 y**		**Neonatal period**	
Blood (µmol/L)							
Glutamate N (P1, 2.5y): 2-118 N (P1, ≥ 5y): 19-95 N (P2): 30-110 N (P3): 27-168	80	34	39	128	194	161	109
Glutamine N (P1, 2.5y): 334-666 N (P1, ≥ 5y): 368-692 N (P2): 370-958 N (P3): 279-1071	726	679	645	793	784	552	520
Proline N (P1, 2.5y): 61-285 N (P1, ≥ 5y): 92-240 N (P2): 107-330 N (P3): 82-367	224	160	217	238	269	202	459
Alanine N (P1, 2.5y): 134-301 N (P1, ≥ 5y): 148-412 N (P2): 131-460 N (P3): 144-450	542	239	285	284	365	243	781
Glycine N (P1, 2.5y): 149-301 N (P1, ≥ 5y): 134-314 N (P2): 224-514 N (P3): 138-381	419	372	503	571	595	250	456
Valine N (P1, 2.5y): 158-310 N (P1, ≥ 5y): 179-327 N (P2): 80-210 N (P3): 62-238	127	100	107	110	111	167	55
Isoleucine N (P1, 2.5y): 37-89 N (P1, ≥ 5y): 47-86 N (P2): 26-80 N (P3): 18-79	33	30	20	25	30	48	14

Leucine N (P1, 2.5y): 68-168 N (P1, ≥ 5y): 86-182 N (P2): 46-160 N (P3): 59-138	57	55	48	46	52	85	28
Lysine N (P1, 2.5y): 113-269 N (P1, ≥ 5y): 90-262 N (P2): 92-310 N (P3): 68-286	223	153	178	189	205	145	162
Blood (mmol/L)							
Lactate N < 1.8 (P1, P3)	4.5					3.7-111	5-17
Pyruvate N < 0.14 (P1) N: 0.06-0.1 (P3)	0.07						0.167
CSF (mmol/L)							
Lactate N < 2.2	1.4						3.1
Pyruvate N < 0.14	0.07						0.167
Urine (µmol/mmol creatinine)							
Lactate N (P1) < 76 N (P3) < 217	94						30160
Pyruvate N: ND							3329
α-oxoglutarate N (P1) < 79 N (P3) < 87	78						465
Succinate N < 97	25						
Fumarate N < 10	4						
3-hydroxybutyrate N < 385						1068	
Glutarate N < 8						39	
2-hydroxyglutarate N < 30						204	
3-hydroxyglutarate N < 8						22	
2-methyl-2,3-dihydroxybutyrate N < 8						28	
Uracil N < 29						57	

Table S3: Enzyme activities in fibroblasts from affected individual LIPT2-P1, LIPT2-P2, LIPT2-P3 and controls.

α-oxoacid dehydrogenases activities measured in fibroblasts showed deficient PDHc and KGDHc activities in P1, P2 and P3 with LIPT2 deficiency and an individual with *LIPT1* mutations. [(a)] adapted from [(7)]

Enzyme activities (pmol/min/mg protein) in fibroblasts

	LIPT2-P1	**Control**	**LIPT1-P** [(a)]	**Control** [(a)]
KGDHc	1400	9700	900	7000
PDHc	276	945	90	1117
Citrate synthase	49400	44500	27000	48000
Isocitrate dehydrogenase	14900	14300	21000	23000

Enzyme activities (nmol/mg protein/min) in isolated fibroblast mitochondria from LIPT2-P2

	LIPT2-P2	**Normal Range**
PDHc	1.7	6.0-19.7
Citrate synthase	173	225-459

Enzyme activities (mU/U citrate synthase) in fibroblasts from LIPT2-P3

	LIPT2-P3	**Normal Range**
PDHc	3.6	9.7-36

Table S4: Polarographic studies in fibroblasts from affected individual LIPT2-P1.

The polarographic assay (nmol O_2/min/mg protein) in LIPT2-P1 fibroblasts showed reduced oxygen consumption using pyruvate as substrate.

	LIPT2-P1	**Control**
Pyruvate+malate	1.9	10.0±1.5
Pyruvate+malate+glutamate	3.2	9.3±1.5

Table S5: Prediction of pathogenic relevance of *LIPT2* mutations

Mutation	**c.89T>C**	**c.314T>G**	**c.377T>G**
Chromosomal location	chr11:74204660A>G	chr11:74204435A>C	chr11:74204372A>C
Protein	p.Leu30Pro	p.Leu105Arg	p.Leu126Arg
1000 Genomes (heterozygous)	1	0	0
ExAC	0	0	0
MutationTaster Score (max. 1)	0.999989713071375	0.999832214029496	0.686451197788724
MutationTaster Prediction	Disease causing	Disease causing	Polymorphism
Provean Score (cutoff<-2.5)	-2.06	-5.96	-3.42
Provean Prediction	Neutral	Deleterious	Deleterious
Polyphen-2 Score (max. 1)	0.897	1	0.985
Polyphen-2 Prediction	Possibly damaging	Probably damaging	Probably damaging